Journal of Nuclear Materials 408 (2011) 224–230

Contents lists available at ScienceDirect

Journal of Nuclear Materials

journal homepage: www.elsevier.com/locate/jnucmat

Densification behaviour and sintering kinetics of ThO_2–4%UO_2 pellet

Joydipta Banerjee [a], T.R.G. Kutty [a,*], Arun Kumar [a], H.S. Kamath [b], Srikumar Banerjee [c]

[a] Radiometallurgy Division, Bhabha Atomic Research Centre, Trombay, Mumbai 400 085, India
[b] Nuclear Fuels Group, Bhabha Atomic Research Centre, Mumbai 400 085, India
[c] Department of Atomic Energy, Anushakti Bhavan, Mumbai 400 001, India

ARTICLE INFO

Article history:
Received 8 September 2010
Accepted 15 November 2010
Available online 20 November 2010

ABSTRACT

ThO_2–⩽4% $^{233}UO_2$ fuel will be the driver fuel for the forthcoming Advanced Heavy Water Reactor (AHWR) in India. Densification behaviour such as shrinkage and shrinkage rates of the green pellets of ThO_2–4wt.% UO_2 (natural 'U') fabricated by Coated Agglomerate Pelletization (CAP) process were studied using a vertical dilatometer at different heating rates. Activation energy of sintering, 'Q', was estimated in the initial stages of sintering by continuous rate of heating (CRH) technique as proposed by 'Wang and Rishi Raj' and 'Young and Cutler'. The sintering mechanism was identified to be as the grain boundary diffusion (GBD) and the average 'Q' value obtained by these two methods were found to be 350 ± 16 kJ/mole and 358 ± 5 kJ/mole, respectively.

1. Introduction

ThO_2 has a higher melting point, better radiation stability, more resistance to chemical interactions, low vapour pressure and has higher thermal conductivity than UO_2. The long-lived minor actinides resulting from fission are generated in much lower quantity with the thorium cycle, especially compared with the plutonium cycle. This ecological advantage is an important argument brought forward these days. The above mentioned properties suggest that thorium based fuels have a greater potential safety and fuel durability than the currently used UO_2 or mixed oxide fuels (MOX). Several reactor concepts based on thorium fuel cycles are under consideration since thorium is much more abundant than uranium. ThO_2 containing around 4% $^{233}UO_2$ along with ThO_2-3 to 4%PuO_2 is the proposed fuel for the forthcoming Indian Advanced Heavy Water Reactor (AHWR). The AHWR is being developed in India with the specific aim of utilizing thorium for power generation since India has vast reserves of thorium.

Coated Agglomerate Pelletization (CAP) process is being developed by Bhabha Atomic Research Centre (BARC), India for the fabrication of ThO_2–UO_2 pellets. The details of this process are given elsewhere [1,2]. Large scale production of these pellets is carried out by the processes involving fabrication of ThO_2 granules, coating with U_3O_8, followed by cold compaction and high temperature sintering. The sintering process is diffusion controlled one whose rate is controlled by the slower moving metal atoms. To determine the underlying physical mechanisms of sintering for a given material system, one must know the kinetic mechanisms by which densification and grain growth occur during sintering. Historically, this has been done experimentally by determining the activation energy for sintering and then comparing that measured value to values reported elsewhere for each possible mass transport mechanism. To obtain the activation energy, one must measure densification rates as a function of temperature, which is all but impossible without the aid of a dilatometer. In this study, the activation energy for sintering was determined using the dilatometric technique. For this, dilatometric runs were carried out on ThO_2–4%UO_2 (composition in wt.%) compacts in Ar–8%H_2 with different heating rates viz. 2, 5, 10 and 15 K/min. The output of this result was used to generate the activation energy for sintering. The activation energy, 'Q', in the initial stage of sintering was estimated by two different methods. The detailed discussion of the methods and the major steps followed for calculation of 'Q' are given in the following paragraphs.

2. Method adopted for determination of sintering activation energy

The kinetics of the non-isothermal densification behaviour has been dealt in detail in literature. A temperature increment method similar for studying the creep mechanism has been suggested by Dorn [3]. The constant rate of heating (CRH) technique has been studied in detail by Young and Cutler [4], Woolfrey and Bannister [5] and Bacmann and Cizeron [6,7] and Wang and Raj [8]. A variant of Wang and Raj's method, which was simpler to formulate, was developed by Dehaudt et al. [9]. Johnson [10] has derived an rate equation for the first ~3.5% of the fractional shrinkage taking into account both volume and grain boundary diffusion by assuming

* Corresponding author. Fax: +91 22 2550 5151.
E-mail address: tkutty@barc.gov.in (T.R.G. Kutty).

0022-3115/$ - see front matter © 2010 Elsevier B.V. All rights reserved.
doi:10.1016/j.jnucmat.2010.11.029

Table 1
Characteristics of ThO_2 and U_3O_8 powders.

Property	ThO_2	U_3O_8
Theoretical density (g/cm^3)	10.00	8.34
Oxygen to metal ratio	2.00	2.66
Specific surface area (m^2/g)	1.67	2.23
Apparent density (g/cm^3)	0.70	1.2
Total impurities (ppm)	<1000	<700

the two sphere shrinkage model. The general equation for the sintering is usually represented by the following relation [9]:

$$y^m = (\Delta L/L_0)^m = K(T)t, \tag{1}$$

where $K(T)$ is the Arrhenius constant and can be expressed as:

$$K(T) = (AD_o\Omega\gamma/TG^{\alpha k}) \cdot \exp(-Q/RT), \tag{2}$$

and $y = \Delta L/L_0$ is the relative shrinkage, ΔL the change in length, L_0 the initial length, k the Boltzmann's constant, t the time, D_o the pre-exponential term of the diffusion coefficient, Ω the atomic volume, γ the free surface energy, G grain size, Q is the activation energy of the process controlling densification, R the universal gas constant, T the temperature and the parameters m, A and α are depend on the geometric shape chosen for the particles and as well as the mechanism responsible for sintering. Here m is a constant which can be expressed as $m = 1/n$, where n is the sintering mechanism parameter whose value depends on the diffusion mechanism. For material transport solely governed by volume diffusion (VD), the value of n varies from 0.40 to 0.50 and where grain boundary diffusion (GBD) is the main diffusion mechanism, the value of n varies from 0.31 to 0.33 [10].

The above Eq. (1) can be rewritten in differential form as:

$$dy/dt = K(T)(y^{1-m}/m). \tag{3}$$

Introducing the expression of $K(T)$ where $K_0 = AD_0\Omega\gamma$ and considering $f(y) = y^{1-m}/m$, we get

$$dy/dt = (K_o/G^{\alpha k}T)\exp(-Q/RT) \cdot f(y). \tag{4}$$

If the experiment is carried out at a constant heating rate, then the relative shrinkage rate equation can be written as

$$dy/dt = (dT/dt) \cdot (dy/dT). \tag{5}$$

Using Eqs. (4) and (5) and taking logarithms of the expression the following equation is obtained [8]:

$$\ln[T \cdot (dy/dT) \cdot (dT/dt)] = -(Q/RT) + \ln K_o - \ln G^{\alpha k} + \ln f(y). \tag{6}$$

If we consider axial and diametrical shrinkages during sintering are homothetic then the relative density, ρ can be expressed in terms of shrinkage, y. Thus densification rate ($d\rho/dt$) can be linked with shrinkage rate (dy/dt) and from equation (6) the following equation is obtained:

$$\ln[T \cdot (d\rho/dT) \cdot (dT/dt)] = -(Q/RT) + \ln K_o - \ln G^{\alpha k} + \ln f(\rho). \tag{7}$$

At same densification level, $\ln[T \cdot (d\rho/dT) \cdot (dT/dt)]$ values were calculated at different temperatures and $\ln[T \cdot (d\rho/dT) \cdot (dT/dt)]$ values are plotted as a function of $1/T$ to find out the activation energy, Q. At same densification level, the grain sizes are identical if same starting powder and same compaction pressure are used. Hence for a constant relative density, the terms $\ln G^{\alpha k}$ and $\ln f(\rho)$ are constant and $\ln K_o$ itself is a constant term.

Young and Cutler [4] have derived the following sintering-rate equations that can quantitatively analyze the densification behaviour at the initial sintering stage measured under CRH technique.

$$d(\Delta L/L_0)/dT \cong [(2.14\gamma\Omega bD_{ob}RT)^{0.33}/(ka^4cQ)](Q/3RT^2) \times \exp(-Q/3RT), \tag{8}$$

$$d(\Delta L/L_0)/dT \cong (5.34\gamma\Omega bD_{ov}RT)^{0.50}/(ka^4cQ)](Q/2RT^2) \times \exp(-Q/2RT). \tag{9}$$

Here, Eqs. (8) and (9) are used for GBD and VD, respectively and a, b and c are particle radius, effective grain boundary width and heating rate (dT/dt), respectively. D_{ob} and D_{ov} represent the constant terms that are given by the following equations:

$$bD_b = bD_{ob}\exp(-Q/RT), \tag{10}$$

$$D_v = bD_{ov}\exp(-Q/RT), \tag{11}$$

where bD_b and D_v are the grain boundary diffusion coefficient and the volume diffusion coefficient respectively. Using shrinkage data measured by CRH techniques, the Q can be estimated from the slope of the plot of $\ln[T^{5/3}d(\Delta L/L_0)/dT]$ or $\ln[T^{3/2}d(\Delta L/L_0)/dT]$ vs. $1/T$ (GBD- or VD-type plot) by assuming GBD or VD [4].

3. Experimental

The green pellets of ThO_2–4%UO_2 for this study were prepared by the CAP process using ThO_2 granules (−40 mesh) and U_3O_8 powder as the starting material. The details of the CAP process are given in Refs. [1,2]. The present work was simulated using natural U instead of ^{233}U. The characteristics of the starting ThO_2 and U_3O_8 powders used in this study are given in Table 1. The green density of the compacts was in the range of 64% of the theoretical density. To facilitate compaction and to impart handling strength to the green pellets, 1 wt.% zinc behenate was added as lubricant/binder during the last 1 h of the mixing/milling procedure. The green pellets were about 12 mm in diameter and around 10 mm in length.

3.1. Dilatometry

The shrinkage behaviour of ThO_2–4%UO_2 green pellets was studied using a high temperature vertical dilatometer (make: Setaram Instrumentation, France; model: Setsys Evoluation 24). Here, the sample rests between the spring loaded push rod and a stopper (end support) inside a sample holder all of which are made of Al_2O_3 material. The change of the length was transmitted through the frictionless push rod to an LVDT transducer. A nominal load of 5 g was chosen to be applied by the push rod over the sample. This was to make sure firm contact by the former over the latter. A calibrated thermocouple (W-5/26% Re) was placed just above the sample to record the sample temperature. The heating rate used for the above studies was 2, 5, 10 and 15 K/min. The samples were heated up to 1923 K using the above heating rate and cooled to room temperature at a rate of 20 K/min. The dilatometric data were obtained as the curves of dimensional change against time and temperature. The shrinkage kinetics experiments were carried out in reducing (Ar–8%H_2) atmospheres at a dynamic gas flow rate of 20 ml/min. The impurity contents of the cover gas used in this study is given in Table 2. The selection of the temperature pro-

Table 2
Impurity contents in the sintering atmospheres (volume ppm).

Sintering atmosphere	Moisture (vppm)	Oxygen (vppm)	CO (vppm)	CO_2 (vppm)	Hydrocarbon (vppm)	N_2 (vppm)	Oxides of N_2 (vppm)
Argon + 8% hydrogen	4	4	1	1	2	10	1

Table 3
Metallic impurities in a typical sintered pellet made by CAP process.

Element	Impurity (ppm)
Si	<110
W	<50
Fe	20
Na	14
Al	9
Mg	5
Co	<5
Mo	<5
Cu	1.0
Cr	<1
Co	<5
Ni	<1
B	<0.6

Table 4
Density and O/M ratio of the sintered ThO_2–UO_2 pellets for different heating rates.

Heating rates (K/min.)	Density (% TD)	O/M ratio
2	89.20	2.00
5	89.18	2.00
10	89.05	2.00
15	87.93	2.00

gramme was made by a computer via data acquisition system. A blank heating was carried out in similar experimental condition where actual samples were heated, called the 'standard run' to find the resultant expansion of sample holder, push rod etc. ('system'). This expansion data of the 'standard run' was subtracted for all subsequent experimental data to obtain the corrected data with respect to the expansion of the 'system'. Table 3 gives the typical impurity contents of a sintered pellet. The density and O/M ratio of the pellets covered in this study are shown in Table 4.

3.2. Characterization

The ThO_2–4%UO_2 pellets were characterized by the following techniques:

- Thermogravimetry
- XRD
- Density
- Metallography

The O/M ratio of the sintered pellet was measured thermogravimetrically and the phase content was estimated using X-ray diffractometry and metallography. The X-ray diffraction patterns of the above sintered pellets were obtained by using CuK_α radiation and graphite monochromator. Accuracy of this equipment is ±5%. For metallography, the sintered pellet as mentioned above was cold mounted in Araldite and ground using successive grades of emery paper. The final polishing was done using diamond paste. The etching is done thermally by holding the sample at 1823 K for 4 h in dynamic Ar–8%H_2 atmosphere. The grain size was determined by the intercept method. The green density was measured geometrically and the sintered density was determined following the Archimedes method.

4. Results

Fig. 1 shows the shrinkage behaviour of ThO_2–4%UO_2 pellet in Ar–8%H_2 for a heating rate of 5 K/min. Here shrinkage (%), ($\Delta L/L_0$) × 100, is plotted against temperature, where L_0 is the initial length of the pellet in the axial direction and ΔL is its increment. The corresponding shrinkage rates, dL/dt, where t is the time, of the above pellet are shown in Fig. 2. Here the shrinkage rate was divided by the initial length of the pellets (L_0) to obtain normalized shrinkage rate (min^{-1}) [$(dL/dt)/L_0$]. From Fig. 1, it is evident that the onset of sintering occurs at around 1173 K for ThO_2–4%UO_2. The onset temperature of shrinkage was determined from the dilatometric curves by extrapolating method. For this, two points are chosen before and after the initial region of the shrinkage vs. temperature plot where sudden slope change is observed. Straight lines drawn along these slopes are extended to find their meeting point. This point is taken as the onset point of sintering. The maximum shrinkage rate for the ThO_2–4%UO_2 pellet was found to occur at around 1333 K for the pellets sintered in Ar–8%H_2.

Fig. 3 shows the shrinkage behaviour of ThO_2–4%UO_2 pellet in Ar–8%H_2 for different heating rate. For comparison, shrinkage behaviour of the above composition for 5 K/min is also included in the above figure. The curves have the familiar shape and generally shifted to higher temperatures with increasing heating rate. It can be noted that the shrinkage obtained at any temperature

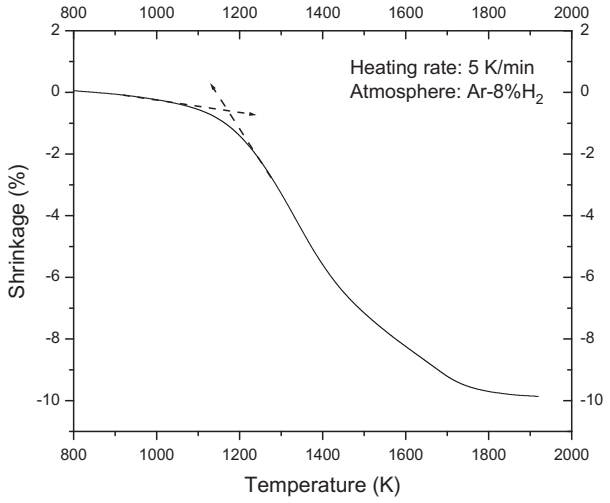

Fig. 1. Shrinkage behaviour of ThO_2–4%UO_2 pellet against temperature in Ar–8%H_2 with the heating rate of 5 K/min.

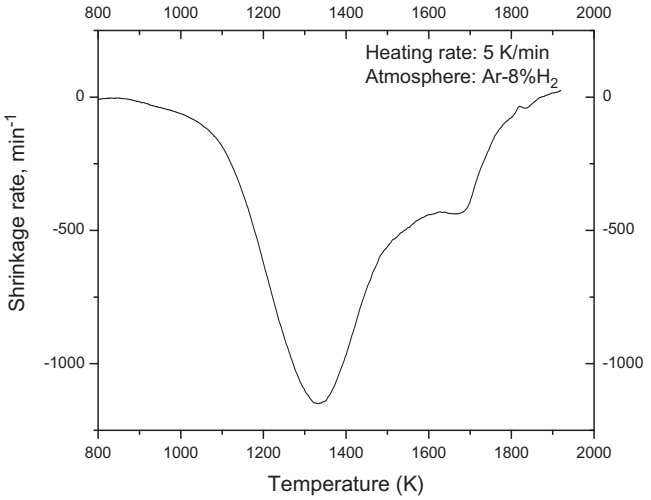

Fig. 2. Plot of shrinkage rate of ThO_2–4%UO_2 pellet against temperature in Ar–8%H_2 with the heating rate of 5 K/min.

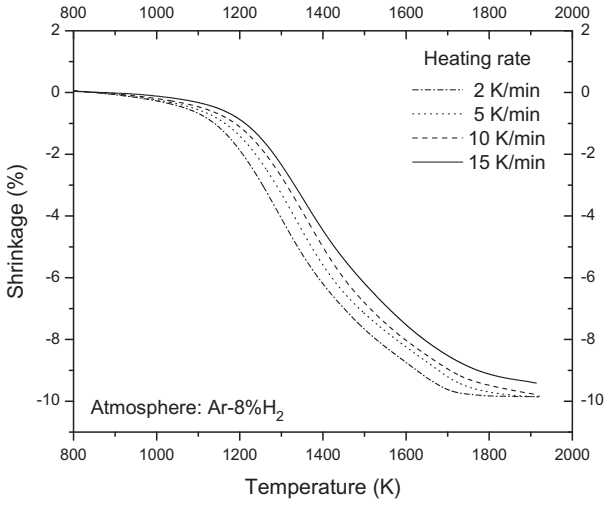

Fig. 3. Shrinkage behaviour of the green pellets against temperature in Ar–8%H_2 heated with different heating rates.

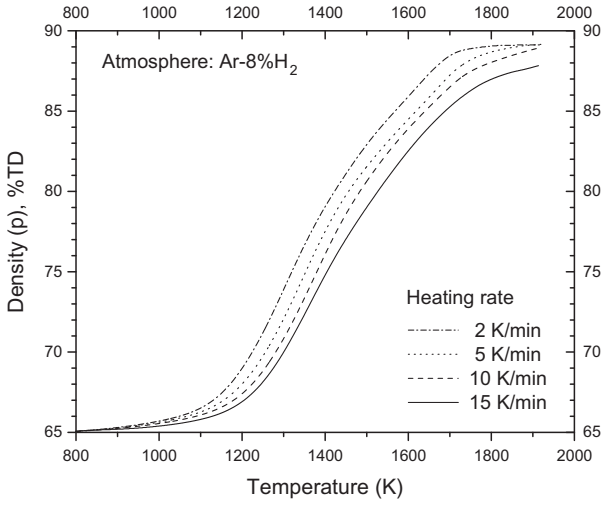

Fig. 5. Plot of relative density attained for the sintered pellets against temperature while heated with different heating rates.

showed a modest but a systematic dependence on heating rate. The maximum shrinkage was found to depend upon the heating rate, the higher the heating rate the lower the sintered density.

It is possible to compute the shrinkage levels at two different temperatures from Fig. 3 and also know the effect of the heating rate on the shrinkage at a particular temperature. The shrinkage at 1473 K was 7.3% for the lowest the heating rate (2 K/min) and was 5.8% for the highest the heating rate (15 K/min). For the same temperature, the shrinkage was 6.4% and 6.8% for the heating rates 10 and 5 K/min, respectively.

Fig. 4 shows the shrinkage rate for ThO_2–4%UO_2 pellets for the different heating rates used in this study. The maximum shrinkage rate shifts to higher temperature with increase in the heating rate. The maximum shrinkage rate was observed at 1300 K for 2 K/min and the same was at 1353 K when the heating rate was increased to 15 K/min.

The shrinkage values of the dilatometric data were converted into percent of theoretical density using the relation [11]:

$$\rho_s = [1/(1 + \Delta L/L_0)]^3 \rho_0. \quad (12)$$

where ρ_s and ρ_0 are the density of the sintered and green pellets, respectively and L_0 is the initial length. Fig. 5 shows the relative density vs. temperature plot for the above pellets. At the highest temperature of 1923 K, a density of around 88% of T.D. was obtained for ThO_2–4%UO_2 when heating rate was 15 K/min. But for 2 K/min, density for the above composition was around 89%.

Fig. 6 shows the typical XRD patterns of both ThO_2–4%UO_2 green and sintered pellets. The XRD pattern of ThO_2–4%UO_2 green pellets clearly shows separate peaks for the initial ThO_2 and U_3O_8 powders indicating the existence of those as separate entities or phases in the green compacts before sintering. The U_3O_8 powders must have got reduced to UO_2 in the Ar–8%H_2 cover gas used during sintering before forming solid solution with ThO_2. This was later confirmed by measurement of the *O*/*M* ratio (Table 4) of the sintered pellets. The X-ray diffraction pattern of the sintered pellet also confirms that the compounds are face centered cubic (fcc) single phased after sintering. The stability of the chemical state of the initial powders was further investigated using thermo-gravimetry (TG) method. The weight loss of the initial green pellet was monitored against temperature where some chips of the green compacts were continuously heated inside TG using the same cover gas as sintering. There was no weight loss observed beyond 1123 K indicating the reduction of U_3O_8 powders was com-

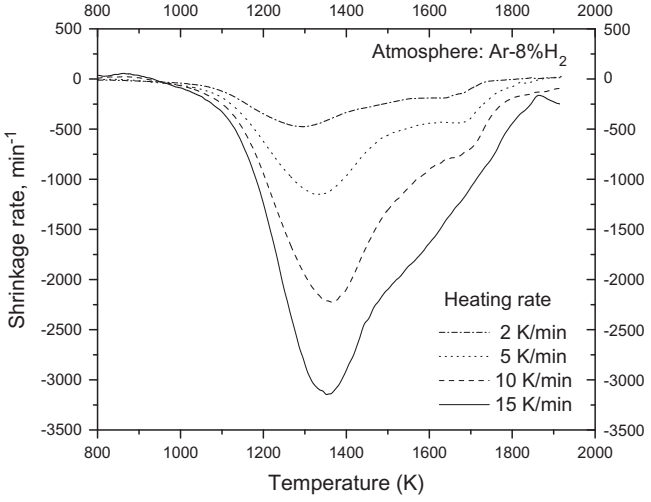

Fig. 4. Plot of shrinkage rates of the green pellets against temperature in Ar–8%H_2 heated with different heating rates.

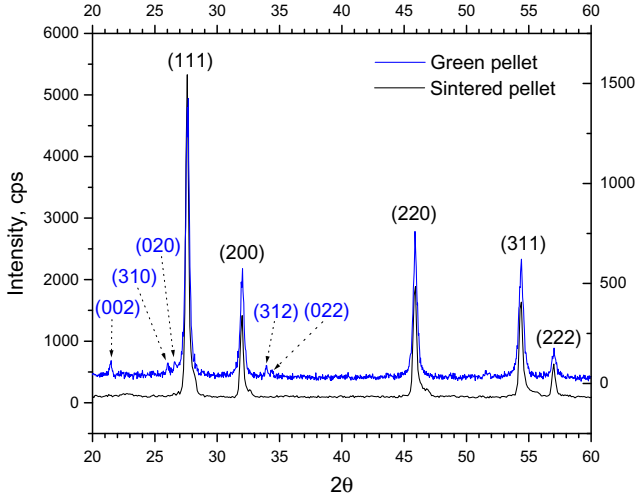

Fig. 6. Typical XRD patterns obtained for the green and sintered ThO_2–4%UO_2 pellet. The XRD pattern of green pellet shows the peaks for ThO_2 as well as U_3O_8.

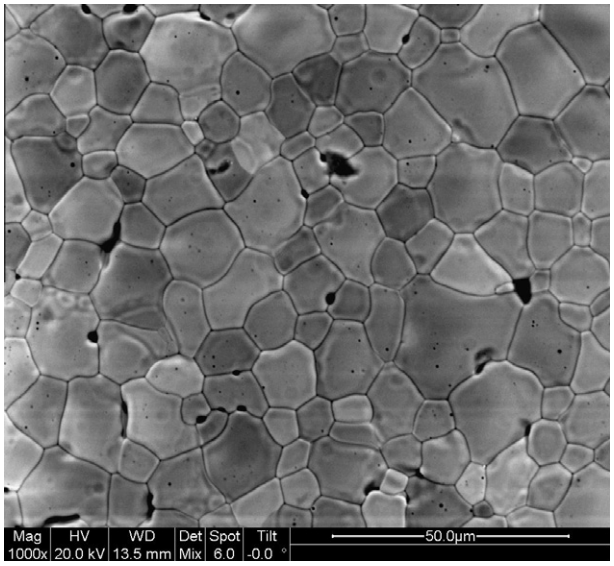

Fig. 7. The microstructure of the sintered pellet as revealed by SEM.

plete below this temperature. All the activation energies in this present study were measured above this temperature. Fig. 7 shows the SEM microstructure of the ThO_2–4%UO_2 pellets. The grains were found to be duplex in nature. The grain size distribution is similar to "rock in sand" structure. There were packets of fine grains uniformly distributed in the matrix. The average size of these fine grains was 1–2 μm. The grain size of the matrix was around 10–11 μm (Fig. 7).

Following the method of Wang and Raj [8], from the density vs. temperature plots of Fig. 5, the slope, $d\rho/dT$ was obtained for a particular density. From this, the values $\ln[T(d\rho/dT)\cdot(dT/dt)]$ was calculated at same density levels and is plotted against $1/T$, which is shown in Fig. 8. From the slope of the above plot, the 'Q' was determined.

Following the method of Young and Cutler [4], activation energy 'Q' was estimated from shrinkage vs. temperature data obtained from any one of the above experiments for a particular heating rate. Q can be estimated from the slope of the plot of $\ln[T^{5/3}d(\Delta L/L_0)/dT]$ or $\ln[T^{3/2}d(\Delta L/L_0)/dT]$ vs. $1/T$ by assuming either GBD or VD respectively. Fig. 9 shows the plot for calculation of Q by this method assuming GBD for a heating rate of 5 K/min.

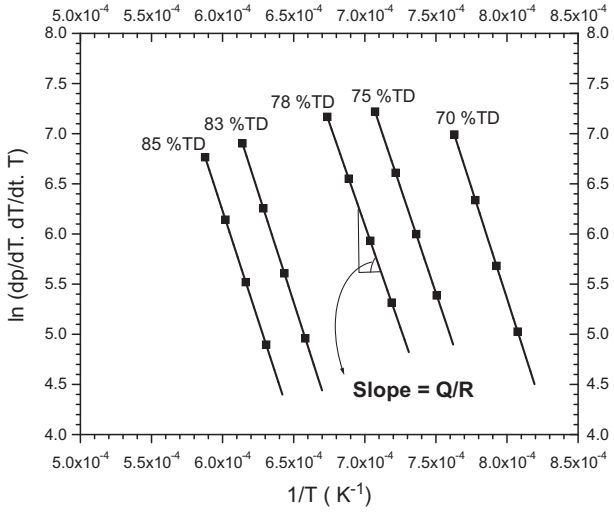

Fig. 8. The plot of $\ln[T\cdot(d\rho/dT)\cdot(dT/dt)]$ vs. $1/T$ for determination of 'Q' using Wang and Rishi Raj method.

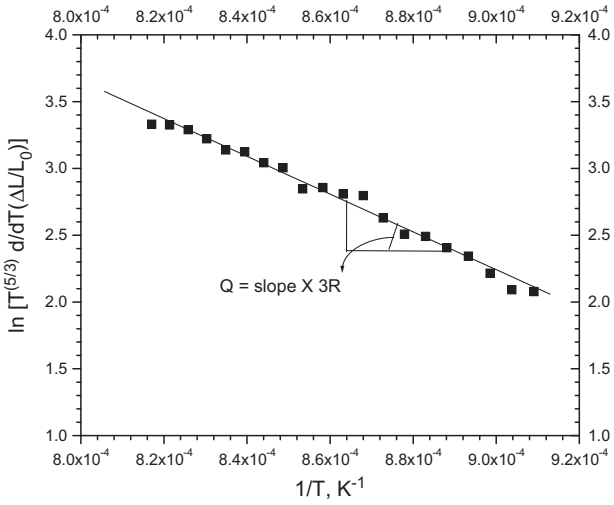

Fig. 9. The plot of $\ln[T^{5/3}d(\Delta L/L_0)/dT]$ vs. $1/T$ for calculation of 'Q' using Young and Cutler method.

'Q' values estimated by Wang and Raj [8] method at different density levels are shown in Table 5. The average 'Q' value thus obtained was 350 ± 16 kJ/mole. Alternately by Young and Cutler [4] method, 'Q' was estimated to be 353 kJ/mole for GBD with the heating rate 5 K/min. The estimation of 'Q' by Young and Cutler method was repeated for heating rates 2 and 10 K/min, when 'Q' was found to be 362 and 361 kJ/mole respectively assuming GBD.

The significant observations are summarized below:

1. From the shrinkage vs. temperature plots for ThO_2–4%UO_2, it can be seen that the onset of sintering is shifted to higher temperatures on increasing the heating rates.
2. The onset of sintering commences at a temperature of ~70 K lower when the heating rate was lowered from 15 K/min. to 2 K/min.
3. The maximum shrinkage rate was found to shift to higher temperature with increase in the heating rate.
4. The maximum density was found to depend upon the heating rate; the higher the heating rate the lower is the sintered density.
5. The microstructure of the ThO_2–4%UO_2 pellet sintered in Ar–8%H_2 showed a duplex grain structure. The grain size distribution is similar to "rock in sand" structure.
6. The activation energy value estimated by Wang and Raj method for ThO_2–4%UO_2 was found to be 350 ± 16 kJ/mole. 'Q' values estimated by Young and Cutler method for the above sample were found to be 358 ± 5 kJ/mole for GBD.

Table 5
'Q' Values estimated by Wang and Raj method.

Density (% TD)	Activation energy, Q, kJ/mole
67	330
68	325
69	338
70	367
72	366
75	351
78	340
80	358
83	366
85	362
Mean (kJ/mole)	350
SD	±15.91

7. The activation energy estimated by Wang and Raj method matches well with that estimated by Young and Cutler method for GBD mechanism.

5. Discussion

Sintering is diffusion dependent, which in turn depends upon the temperature. Temperature controls the rate of atomic motion, and higher temperature gives more rapid sintering. Diffusion can occur by several paths. The total mass transport can be divided into two transport mechanisms, namely surface transport and bulk transport [12–14]. The important distinction between the two mechanisms is related to shrinkage or the dimensional changes occurring. Surface transport gives no dimensional changes while bulk transport (volume diffusion, grain boundary diffusion, plastic flow, and viscous flow) produces shrinkage; i.e. for densification to occur, the mass must originate form the particle interior with deposition at the neck. Hence the densification occurring during sintering can be correlated to the diffusion time involved in it [15,16].

From the sintering-rate equations used for CRH techniques, only the activation energy for diffusion can be determined experimentally. However, the diffusion mechanism cannot be determined using the CRH techniques. Conventionally, this can be determined experimentally by analyzing the isothermal shrinkage process. Matsui et al. [17] derived an analysis method used for CRH techniques by which not only the activation energy but the diffusion mechanism for the initial stage of sintering can be determined experimentally. Using the Eq. (7), and from the slope (S_1) of $\ln[T\cdot(d\rho/dT)\cdot(dT/dt)]$ vs. $1/T$ plot for the same density, Matsui et al. [17] derived an expression for the activation energy as:

$$Q = RS_1 \tag{13}$$

Similarly, using the procedure of Young and Cutler and using Eqs. (8) and (9), for GBD or VD-type plot, the slope S_2 was determined [17] and an expression for the activation energy was derived as:

$$Q/m = RS_2 \tag{14}$$

where the value of m depends on diffusion mechanism ($m = 2$ for VD; and $m = 3$ for GBD). In the initial stages of sintering, the two Q values of the above equations are equal. Combining these two, we get,

$$m = Q/(Q/m) = S_1/S_2 \tag{15}$$

The above equation implies that, using the sintering-rate equations of Wang and Raj and Young and Cutler, the diffusion mechanism for the initial stages of sintering can be determined experimentally using CRH techniques. Matsui et al. [17] suggested that the above analysis becomes valid only if the analysis were performed at a fractional shrinkage of <4%. When the fractional shrinkages of <4% is satisfied, the influences of density and particle size on the Q and Q/m are negligibly small. The sintering mechanism parameter, n, thus calculated in the present investigation was found to vary between 0.32 and 0.33 indicating that that prevailing sintering mechanism for ThO_2–4%UO_2 was GBD.

Results on the diffusion of Th and U in ThO_2 have been reported by various authors [18–24], showing, however, an unusually big scatter. King [18] suggested that most of these data might be influenced by grain boundary or dislocation diffusion, and that volume diffusion proceeds at much lower rates than previously thought. The diffusion coefficient for uranium, D_U, in reactor grade ThO_2 was determined by many authors. Matzke [19] has reported the value of D_U in ThO_2 at 1673 K and 1823 K as 2×10^{-14} cm^2/s and 3×10^{-13} cm^2/s, respectively. Olander [20] determined the volume and grain boundary diffusion coefficients in ThO_2–UO_{2+x} mixed oxides, which were deduced from the concentration distributions established by preferential evaporation of UO_3 during air-annealing of a specimen at 1923 K. The volume diffusion coefficient for $U_{0.1}Th_{0.9}O_{2.05}$ and $U_{0.25}Th_{0.75}O_{2.125}$ was found to be 3×10^{-14} cm^2/s and 8×10^{-13} cm^2/s, respectively. Matzke [21] has studied the diffusion of U in ThO_2 by conducting very extensive diffusion anneals using both polycrystals and single crystals in a broad temperature range. He reported that volume diffusion is less predominant below $0.6T_m$ for ThO_2 and was found be of the order of $\sim 10^{-18}$ cm^2/s at 1873 K. Matzke [21] suggested that in polycrystalline ThO_2, grain boundary penetration dominates. The grain boundary diffusion coefficients for ThO_2 are 10^{-10} cm^2/s to 10^{-9} cm^2/s at 1673 K to 1773 K. And at 2273 K, the grain boundary diffusion coefficients are of the order of 10^{-7} cm^2/s to 10^{-6} cm^2/s for the above material. Hence, it is evident that for the actinide oxides diffusion coefficient (grain boundary) are about few orders higher than the volume diffusion. From the data for the diffusion of U and Th in ThO_2 of Matzke [21], the grain boundary diffusion coefficients are compared for 1923 K and 1673 K and found that the grain boundary diffusion coefficient at 1923 K is about 100 times higher than that at 1673 K.

In this study, the activation energy for the initial stage of sintering of ThO_2–4%UO_2 was determined by two different methods. The 'Q', determined using Wang and Raj method, was found to be 350 ± 16 kJ/mole. Alternately, using Young and Cutler method, 'Q' was estimated to be 358 ± 5 kJ/mole for GBD. The activation energy estimated by Wang and Raj method matches well with that estimated by Young and Cutler method for GBD mechanism. The activation energy for the diffusion in ThO_2–UO_2 system has been measured by many authors [22–24]. Hawkins and Alcock [22] found activation energy of 2.55 eV for polycrystalline thoria, whereas King [18] and Matzke [19] reported much higher values of 6.48 eV and 6.5 eV, respectively. Recently Kutty et al. [25] estimated activation energy of ThO_2–2%U_3O_8 pellet made by powder metallurgy route using master sintering curve approach. They obtained activation energy of the above composition as 500 kJ/mole. Furuya [23] has shown that the activation energy of lattice diffusion of uranium in ThO_2 is smaller than that in ThO_2–UO_2 solid solution. This behaviour is explained by the difference of lattice spacing in the two substances. ThO_2 and UO_2 form a complete series of solid solutions and the lattice spacing decreases with increasing concentration of UO_2. The small lattice spacing in ThO_2–UO_2 cause the potential barrier to increase which results in a high activation energy, compared with ThO_2.

Aiybers [24] studied the first-stage sintering of $(U_{0.8},Th_{0.2})O_{2+x}$, $(U_{0.05},Th_{0.95})O_{2+x}$ using a dilatometer. With the aid of shrinkage curves, the apparent activation energy and the diffusion coefficients are calculated for reducing atmospheres. He has shown that both the atmosphere and the composition affected the activation energy. He has reported that the value of n is about 0.46 and 0.3 for reducing and CO_2 atmosphere, respectively. This means that the sintering mechanism has changed according to the atmosphere. In CO_2 atmosphere U atoms diffuse approximately 1000 times faster than the case of reducing atmosphere. The diffusion work on $(U, Pu)O_2$ by El-Sayed Ali [26] has shown almost identical results, indicating volume diffusion in reducing atmosphere and grain boundary diffusion for CO_2 atmosphere as the sintering mechanism. With the aid of the shrinkage curves, the apparent activation energy of $(U_{0.8},Th_{0.2})O_{2+x}$ for the initial stages of sintering for is calculated to be about 339 kJ/mole in reducing atmosphere and 294.7 kJ/mole in oxidizing atmosphere. The apparent activation energy of ThO_2–4%UO_2 for the initial stages of sintering obtained in this study using dilatometry has shown that the grain boundary diffusion is the rate controlled mechanism for the initial stage of sintering. Our results are contrary to the results reported in [24,26] where authors had reported that the volume diffusion is the rate controlling mechanism in reducing atmosphere for ThO_2–UO_2 pellets. The reason for the change of mechanism may

be correlated to the microstructure of ThO_2–UO_2 pellets obtained in this study. The microstructure of ThO_2–UO_2 pellet prepared by CAP process showed a ''rock in sand'' type structure. There were colonies of fine grains which were surrounded by large grained areas. The average size of these fine grains was 1–2 μm compared to the grain size of the matrix which was around 10–11 μm. Therefore, the presence of finer grain size might have promoted grain diffusion over the volume diffusion as the rate controlling mechanism.

6. Conclusions

ThO_2–4%UO_2 pellets have been fabricated by the newly developed CAP route using ThO_2 and U_3O_8 powders as the starting materials. The sintered pellets were characterized in terms of microstructure and the sintering kinetics was evaluated using dilatometry by CRH technique. The shrinkage behaviour of ThO_2–4%UO_2 pellets was studied using a high temperature using the heating rates of 2, 5, 10 and 15 K/min. The following conclusions are drawn:

1. The activation energy value estimated by Wang and Raj method for ThO_2–4%UO_2 was found to be 350 ± 16 kJ/mole.
2. The same estimated by Young and Cutler method for the above sample was found to be 358 ± 5 kJ/mole for GBD.

The sintering mechanism parameter, n, was found to vary between 0.32 and 0.33 indicating that that prevailing sintering mechanism for ThO_2–4%UO_2 was GBD.

Acknowledgements

The authors wish to express their gratitude to Dr. Jose Panakkal, Head, Advanced Fuel Fabrication Facility, Tarapur, Bhabha Atomic Research Centre for the supply of green pellets fabricated by CAP process for the present study. Thanks are also given to Mr. Abhijit Ghosh, Materials Processing Division, Materials Group, Bhabha Atomic Research Centre for his useful discussion and suggestions.

References

[1] T.R.G. Kutty, K.B. Khan, P.S. Somayajulu, A.K. Sengupta, J.P. Panakkal, Arun Kumar, H.S. Kamath, J. Nucl. Mater. 373 (2008) 299.
[2] T.R.G. Kutty, K.B. Khan, P.S. Somayajulu, A.K. Sengupta, J.P. Panakkal, Arun Kumar, H.S. Kamath, J. Nucl. Mater. 373 (2008) 309.
[3] J.E. Dorn, in: R. Maddin (Ed.), Creep and Recovery, American Society for Metals, Cleveland, OH, 1957, p. 255.
[4] S. Young, B. Cutler, J. Am. Ceram. Soc. 53 (12) (1970) 659.
[5] J.L. Woolfrey, M.J. Bannister, J. Am. Ceram. Soc. 55 (8) (1972) 390–394.
[6] J.J. Bacmann, G. Cizeron, J. Nucl. Mater. 33 (1969) 271.
[7] J.J. Bacmann, G. Cizeron, J. Am. Ceram. Soc. 51 (1968) 209.
[8] J. Wang, R. Raj, J. Am. Ceram. Soc. 73 (5) (1990) 1172–1175.
[9] Ph. Dehaudt, L. Bourgeois, H. Chevrel, J. Nucl. Mater. 299 (2001) 250.
[10] D.L. Johnson, J. Appl. Phys. 40 (1969) 192.
[11] T.R.G. Kutty, P.V. Hegde, K.B. Khan, S.N. Pillai, A.K. Sengupta, G.C. Jain, S. Majumdar, H.S. Kamath, D.S.C. Purushotham, J. Nucl. Mater. 305 (2002) 159.
[12] F. Thummler, W. Thomma, Metall. Rev. 115 (1967) 69.
[13] R.L. Coble, J.E. Burke, in: J.E. Burke (Ed.), Progress in Ceramic Science, vol. 3, Pergamon, Oxford, 1963, p. 197.
[14] M. Mayo, Int. Mater. Rev. 41 (3) (1996) 85.
[15] W.D. Kingery, M. Berg, J. Appl. Phys. 26 (10) (1955) 1205–1212.
[16] R.L. Coble, J. Am. Ceram. Soc. 41 (2) (1958) 55–62.
[17] Koji Matsui et al., J. Am. Ceram. Soc. 88 (12) (2005) 3346–3352.
[18] A.D. King, J. Nucl. Mater. 38 (1971) 347.
[19] Hj. Matzke, J. Nucl. Mater. 21 (1967) 190.
[20] D.R. Olander, J. Nucl. Mater. 144 (1987) 105.
[21] Hj. Matzke, J. Phys. Colloque C7 37 (1976) 452.
[22] R.J. Hawkins, C.B. Alcock, J. Nucl. Mater. 26 (1967) 112.
[23] H. Furuya, J. Nucl. Mater. 26 (1968) 123.
[24] M.T. Aybers, J. Nucl. Mater. 210 (1994) 73.
[25] T.R.G. Kutty, K.B. Khan, P.V. Hegde, A.K. Sengupta, S. Majumdar, H.S. Kamath, Science of Sintering 35 (2003) 125.
[26] M.M. El-Sayed Ali, Etude Du Stade Initiale De Frittage Des Oxydes D'Actinides: UO_2, PuO_2, et De Leurs Melanges, PhD. Thesis, 1979.